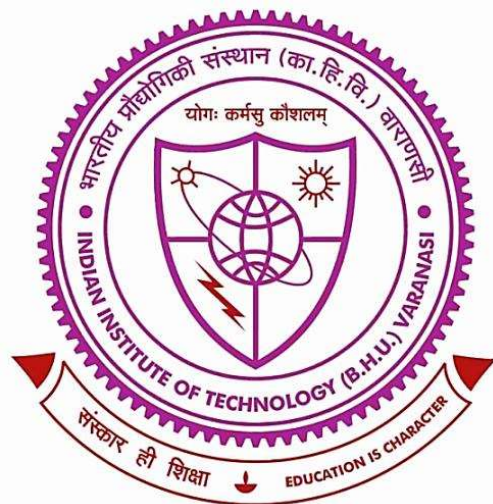


# **Zeolitic Imidazolate Framework-Derived Layered Double Hydroxides for Electrochemical Water Oxidation**



**Thesis submitted in partial fulfilment for the  
Award of Degree  
Doctor of Philosophy**

**by  
Priyanka Maurya**

**DEPARTMENT OF CHEMISTRY  
INDIAN INSTITUTE OF TECHNOLOGY  
(BANARAS HINDU UNIVERSITY)  
VARANASI-221005  
INDIA**

**Roll No. 18051012**

**Year 2025**

---

---

# COPYRIGHT TRA

---

---

Title of the Thesis: **Zeolitic Imidazolate I**  
**for Electrochemical Water Oxidation.**

Name of the Student: **Priyanka Maurya**

**COPYRIGHT**

---

---

CER

---

---

It is certified that the work contained in

**Derived Layered Double Hydroxides for**

**Maurya** has been carried out under my

elsewhere for a degree.

It is further certified that the student

Examination, Candidacy, and SOTA for

---

---

## DECLARATION

---

---

I, "Priyanka Maurya", certify that the work mentioned above is my  
bonafide work and carried out by me under the supervision of  
"July-2018" to " June-2024", at the Department of  
Technology, (BHU), Varanasi. The matter mentioned above is not  
the award of any other degree/diploma. I declare that I have not  
credits to the research workers wherever their work is mentioned.  
I further declare that I have not willfully copied or plagiarized any

CERT

Certified that the work contained in the thesis  
**Layered Double Hydroxides for Electro**  
**Maurya** has been carried out under my super  
mandatory requirement of TWO quality publi

It is further certified that the two publicati  
**Maurya** have been published in the Journals

(a) SCI

(b) SCI Extended

(c) SCOPUS

(d) Non-indexed journals-

(Only in special cases)

(\* Please enclose DPGC resolution in this

# Contents

---

<b>Title</b>	<b>Page No.</b>
Title of thesis	<b>i</b>
Dedication	<b>ii</b>
Certificate	<b>iii</b>
Declaration by the candidate and certificate by the supervisor	<b>iv</b>
Copyright transfer certificate	<b>v</b>
Acknowledgment	<b>vi</b>
Contents	<b>viii</b>
List of Figures	<b>xii</b>
List of Schemes	<b>xix</b>
List of Tables	<b>xx</b>
List of Symbols/Abbreviations	<b>xxii</b>
Preface	<b>xxiv</b>
<b>Chapter-1: General Introduction</b>	<b>1-34</b>
1. Introduction	<b>2</b>
1.1. Electrochemical water oxidation	<b>3</b>
1.2. Electrocatalytic kinetic parameters for OER	<b>3</b>
1.2.1. Overpotential ( $\eta$ )	<b>4</b>
1.2.2. Tafel slope	<b>4</b>
1.2.3. Faradaic efficiency	<b>5</b>
1.2.4. Turnover frequency (TOF)	<b>6</b>
1.2.5. Stability	<b>7</b>
1.2.6. Electrochemical active surface area	<b>8</b>
1.2.7. Electrochemical impedance spectroscopy (EIS)	<b>9</b>
1.3. Electrocatalysts for OER based on transition metal	<b>10</b>
1.4. Layered double hydroxides (LDHs)	<b>12</b>
1.5. Metal-organic framework-derived LDHs for OER	<b>18</b>

---

1.6. Zeolitic imidazolate frameworks (ZIFs)	19
1.6.1. ZIFs as OER electrocatalysts	21
1.6.2. ZIF-67 derived LDHs for OER	22
1.7. Motivation and objective of thesis	23
1.8. References	26
<b>Chapter-2: Metal-Organic Framework Derived Hollow Cobalt Vanadium Layered Double Hydroxide Nanocages for Efficient Electrochemical Water Oxidation</b>	<b>35-50</b>
2.1. Introduction	36
2.2. Chemicals	38
2.3. Instruments	38
2.4. Experimental	38
2.4.1. Synthesis of ZIF-67	38
2.4.2. Synthesis of V <sub>x</sub> Co-LDH	39
2.4.3. Activation of nickel foam	39
2.4.4. Deposition of catalysts on nickel foam	39
2.5. Result and discussion	40
2.5.1. Characterization of catalysts	40
2.5.2. Electrochemical activity	43
2.6. Conclusion	46
2.7. References	46
<b>Chapter-3: Iron(III) ion-Facilitated Conversion of ZIF-67 to a Self-supported Fe<sub>x</sub>Co-Layered Double Hydroxide for Improved Water Oxidation</b>	<b>51-72</b>
3.1. Introduction	52
3.2. Chemicals	53
3.3. Instruments	53
3.4. Experimental	53

---

3.4.1. Activation of nickel foam	53
3.4.2. Synthesis of cobalt hydroxide carbonate template on nickel foam	54
3.4.3. Synthesis of iron cobalt hydroxide carbonate template on nickel foam (Fe <sub>0.4</sub> Co-HC@NF	54
3.4.4. Synthesis of ZIF-67@NF	54
3.4.5. Synthesis of Fe <sub>0.4</sub> Co-ZIF-67@NF	55
3.4.6. Synthesis of Fe <sub>0.4</sub> Co-LDH@NF	55
3.4.7. Synthesis of Co-LDH@NF	55
3.4.8. Synthesis of ZnCo-LDH@NF	55
3.5. Results and discussion	56
3.5.1. Characterizations of the catalyst	56
3.5.2. Electrochemical activity	60
3.6. Conclusion	69
3.7. Reference	69
<b>Chapter-4: Electrochemical Fe(III) ion Incorporation in the Structure of ZIF-67- Derived Co-Layered Double Hydroxide Boosts Water Oxidation Activity</b>	<b>73-85</b>
4.1. Introduction	74
4.2. Chemicals	75
4.3. Instruments	76
4.4. Experimental	76
4.4.1. Activation of nickel foam	76
4.4.2. Synthesis of ZIF-67@NF	76
4.4.3. Electrochemical reconstruction of ZIF@NF precatalyst into FeCo-LDH-x and Co-LDH	76
4.5. Results and discussion	76
4.5.1. Characterizations of the catalyst	76
4.5.2. Electrochemical activity	80
4.6. Conclusion	83
4.7. Reference	84

---

<b>Chapter-5: The 4f-2p-3d Orbital Overlap Formed in a CeO<sub>2</sub>/CeCo-LDH Heterostructure Derived from a Metal-Organic Framework for Improved Water Oxidation</b>	<b>86-106</b>
5.1. Introduction	87
5.2. Chemicals	89
5.3. Instruments	89
5.4. Experimental	89
5.4.1. Activation of nickel foam	89
5.4.2. Synthesis of cobalt hydroxide carbonate template on nickel foam (Co-HC@NF)	90
5.4.3. Synthesis of ZIF-67@NF	90
5.4.4. Synthesis of CeCo-2	90
5.4.5. Synthesis of CeO <sub>2</sub> +Co-LDH@NF	90
5.4.6. Synthesis of CeCo-LDH	90
5.4.7. Synthesis of Co-LDH	91
5.5. Results and discussion	91
5.5.1. Characterizations of the catalyst	91
5.5.2. Electrochemical Activity	96
5.6. Conclusion	102
5.7. Reference	103
<b>Chapter-6: Conclusion and future prospective</b>	<b>107-111</b>
6.1. Summary	108
6.2. Future scope and perspective	109
List of publications	111

---

---

## Preface

---

---

The electrochemical oxygen evolution reaction (OER), an anodic half-reaction of water electrolysis, has attained enormous attention in the field of energy conversion. However, OER is a bottleneck for the large-scale production of hydrogen gas due to the involvement of high energy reaction intermediate following a four-proton and four-electron transfer mechanism. Therefore, the OER kinetics is sluggish and it becomes a thermodynamically unfavorable reaction. OER requires additional energy input to cross the high energy barrier. Recently, efforts have been provided to develop transition metal-based electrocatalysts for efficient electrochemical OER. Among different OER active materials, layered double hydroxides (LDHs) have emerged as one of the most outstanding electrocatalysts because of the flexibility in their composition and structure and facile fabrication techniques. In this reference, Co-LDHs have been considered to show promising OER activity but their OER activity is constrained due to the low Gibbs free binding energy of \*O on Co-sites and their low electronic conductivity.

Recently, MOF-derived self-supported LDHs have come out as one of the most promising groups of electrocatalysts because of their unique layered structure and potent electrocatalytic activity. In this context, we have utilized self-supported ZIF-67 (zeolitic imidazolate framework, a subclass of metal organic framework, MOF) as the precatalyst to form the active catalysts. ZIF-67-derived LDHs have high surface area and tunable pore structure, which make them suitable OER catalysts.

In addition to this, the incorporation of high-valent metals in Co-LDHs can greatly enhance the OER performance. Simultaneously, the use of a self-supported catalyst on a conductive substrate can enhance the electronic conductivity and strengthen the interaction between catalysts

and support which improves the activity and stability. Therefore, in this thesis, we have explored the self-supported and heterometal-doped Co-LDHs to attain the required OER catalytic activity.

**Chapter-1** demonstrates the objectives of the thesis work looking at progress in this field. In this chapter, we have covered the principles of electrochemical water oxidation, its significance in the field of energy conversion and storage, and its evaluation parameters. Further, we have discussed the previously reported MOF-derived LDHs for OER along with various shortcomings in this field. We have discussed the advantages of using ZIF-67 as the precursor for the synthesis of OER catalysts.

**Chapter-2** demonstrates the synthesis of noble-metal free V-doped Co-LDHs ( $V_x\text{Co-LDH}$ ) hollow nanocages, synthesized from ZIF-67. ZIF-67 was converted into LDH along with the incorporation of vanadium when treated with  $\text{VCl}_3$ . The V doping has been found to be crucial to enhance the OER activity of Co-LDH in the alkaline medium. The effect of changing the amount of V on the activity of  $V_x\text{Co-LDH}$  was also studied and it was observed that all  $V_x\text{Co-LDH}$  exhibited better OER activity than Co-LDH while the activity of  $V_{0.2}\text{Co-LDH}$  was found to be best among all the synthesized  $V_x\text{Co-LDH}$ s.  $V_{0.2}\text{Co-LDH}$  required only 280 mV of overpotential to produce  $100 \text{ mA cm}^{-2}$  of current density with stability for 24 h.

**Chapter-3** explains the Lewis acid-assisted hydroxylation of ZIF-67 to form  $\text{Fe}_x\text{Co-LDH}$  nanosheets via hydrothermal technique. The most appropriate reaction condition for the complete reconstruction and optimal OER activity has been determined. The effect of variation in the quantity of Fe(III) on the OER activity of  $\text{Fe}_x\text{Co-LDH}$  has been explored where it was found that

Fe<sub>0.4</sub>Co-LDH exhibited the best OER activity. The enhanced electrochemical OER activity of ultrathin nanosheets has also been compared with Co-LDH, ZnCo-LDH, and hydrothermally synthesized Fe<sub>0.4</sub>Co-HC.

In **Chapter-4**, we have shown electrochemical reconstruction of ZIF-67 during anodic water oxidation resulting in the formation of FeCo-LDH-x [Fe-Co(OH)<sub>2</sub>/Co(O)OH] (where x = 1, 2, 3, 4, 5). The Fe(III)-ions, present in the electrolyte solution, are introduced in the structure of the active catalyst during the anodic reconstruction of ZIF-67. Electrochemically derived FeCo-LDH-x demonstrates high electrochemical surface area, exposed active sites, atomic-level thickness, and adjusted structural and electronic features to improve the OER activity. The activity of all FeCo-LDH-x was found to be better than that of as synthesized Co-LDH-3. Among the synthesized catalysts, FeCo-LDH-3 exhibited the best OER activity generating 50 mA cm<sup>-2</sup> current density at 180 mV overpotential and with the lowest Tafel slope value and charge transfer resistance.

**Chapter-5** demonstrates a facile technique for the synthesis of a self-supported heterostructure catalyst system CeO<sub>2</sub>/Ce-Co-LDH (CeCo-x, where, x= 1, 2, 3) using nickel foam supported ZIF-67. The precursor was treated with various amount of Ce(NO<sub>3</sub>)<sub>3</sub>.9H<sub>2</sub>O by hydrothermal technique. During hydrothermal treatment, the insertion of Ce into Co-LDH resulted in 4f-2p-3d orbital overlap along with the formation of heterojunction between CeO<sub>2</sub> and CeCo-LDH. Out of all synthesized CeCo-x catalysts, CeCo-2 demonstrated excellent OER activity as it produces 50 mA cm<sup>-2</sup> current density at a very low overpotential of 220 mV. 4f-2p-3d orbital overlap modulated the electronic structure and the heterostructure regulated the transportation of charges during the OER process. The 4f-2p-3d orbital overlap demonstrated the more proficient delocalization of  $\pi$ -

electron density over metal center via oxide bridging in comparison to 3d-2p-3d overlap. Thus, CeO<sub>2</sub>/Ce-Co-LDH heterostructures exhibited excellent OER performance and stability.

**In Chapter-6** we have presented a succinct overview of the scientific contributions made in this thesis and summarized our findings, which provide valuable insights for the development of ZIF-67 derived new efficient electrocatalysts for electrochemical energy conversion. We have also explored the future prospects of these research endeavors.

# *Acknowledgment*

In this moment of reminiscence, I would like to thank everyone who has helped me during my Ph.D. journey at IIT (BHU). I see it as a happy and modest act, in addition to my moral duty, to express my genuine gratitude to everyone.

First and foremost, I would like to express my gratitude to my esteemed supervisor, Dr. Arindam Indra, whose invaluable supervision, unwavering support, patience, motivation, profound knowledge and expert guidance have been proved as cornerstones throughout my pursuit of Ph.D. degree. His guidance served as a beacon to guide me and improved the quality of my research and thesis writing. I am incredibly grateful for the chance to have such a dedicated mentor and advisor.

I am incredibly grateful to HOD, Prof. Sundaram Singh, and Ex-HOD, Prof. Y. C. Sharma, Department of Chemistry, IIT (BHU), for providing me the resources and their constant support during my research period. My special appreciation goes to my RPEC members, Prof. Kamdeo Mandal, Department of Chemistry, IIT (BHU) and Prof. Pralay Maiti, Department of School of Material Science and Technology, IIT (BHU), for their perceptive advice, constant guidance, and considerate assistance during my research work. I express my sincere gratitude to all the faculty members of my department, for their encouragement and assistance. I extend my sincere gratitude to all non-teaching staff (Mr. Rambish, Mr. Neeraj, Mr. Abhishek and Mr. Amit) of the Chemistry Department of IIT(BHU), because this work could not be accomplished without their technical assistance.

I also gratefully acknowledge the DST-INSPIRE for the financial support in the form of JRF and SRF. I express my gratitude to CIFC, IIT (BHU), Varanasi, for providing the resources required to do several sample characterisations.

I am indebted to my lab mates, Dr. Ved Vyas, Mr. Deepak Kumar, Mr. Vishesh Kumar, Mr. Toufik Ansari, Deepak Kumar Ray, Vijay Patel and Harshit Gupta for their intellectually

fascinating conversations and the camaraderie that enriched the last five years. I feel incredibly fortunate to offer my heartfelt gratitude to my friend, mentor, and senior, "Dr. Abhay Narayan Singh", Department of School of Material Science and Technology, IIT (BHU), for all his support and insightful advice.

I would like to thank my friends Ms. Garima Pandey, Ms. Aditi, and Dr. Swati Chauhan for their companionship, constant motivation and love. I am deeply grateful to my beloved husband, Mr. Rohit Kumar Maurya, for his unwavering support, love, laughter, and motivation. His encouragement has kept me focused and made this project possible, especially during the challenging times. I wish to express my heartfelt gratitude to everyone who has offered their support in various ways during my time at the Indian Institute of Technology (Banaras Hindu University), Varanasi, India. I am also grateful for the negative experiences, as they have taught me valuable life lessons and contributed to my growth.

I express my heartfelt thanks to my most loving and caring Grandmother, Smt. Kamla Devi and my grandfather, Late Ram Adhar Maurya, for being the best storytellers, inspiring me to study and teaching me about life. I am extremely thankful to my loving mother, Smt. Asha Maurya and father Sri Panna Lal Maurya for their unconditional love and sacrifices. I am also very grateful to my loving and caring brothers, Mr. Pradip Kumar Maurya, Mr. Prashant Kumar Maurya, Mr. Piyush Kumar Maurya and Mr. Praveen Kumar Maurya, for their unwavering support and love that helped me many times in many ways.

I am also grateful to my loving and supportive sisters-in-law, Mrs. Nisha Maurya, Mrs. Arti Maurya, and Mrs. Pooja Maurya, for their love, blessings, support and motivation.

I am also blessed with my loving nieces, Avisha, Kashvi, and Pravya, who bring immense joy to my life.

**Date: 08/07/2025**

**Priyanka Maurya**

**Place: Varanasi**

# List of Figures

---

<b>Figure No.</b>	<b>Title</b>	<b>Page No</b>
<b>Figure 1.1.</b>	(a) Schematic representation for the electrochemical water splitting process, depicting the anodic OER and cathodic HER; (b) Graph displaying the relationship between potential and current density for OER and HER.	<b>3</b>
<b>Figure 1.2.</b>	Displays the different types of OER kinetic parameters.	<b>5</b>
<b>Figure 1.3.</b>	(a) Cyclic voltammetry curve illustrating OER; (b) Tafel plots displaying electrocatalyst performance for OER; (c) Cyclic voltammetry profile demonstrating redox peaks for determining surface active sites of an electrocatalyst, (d) ( $C_{dl}$ ) plot for calculating the electrochemically active surface area (ECSA); (e) Stability test using chronoamperometry for an OER electrocatalyst; (f) Nyquist plot obtained from electrochemical impedance spectroscopy.	<b>9</b>
<b>Figure 1.4.</b>	Graph showing the possible approaches for improving performance for OER using transition metal-based electrocatalyst.	<b>12</b>
<b>Figure 1.5.</b>	Schematic illustration for Strategies for modulation of LDH-based electrocatalysts towards HER and OER.	<b>14</b>
<b>Figure 1.6.</b>	schematic representation for the synthesis of LDHs from different types of MOFs.	<b>19</b>
<b>Figure 1.7.</b>	Illustration of structure of ZIF and similarity with zeolite.	<b>20</b>
<b>Figure 1.8.</b>	Demonstrates the advantages of the ZIF-67 as OER catalysts.	<b>21</b>

- Figure 1.9.** Demonstrates the chapter-wise objectives of the thesis. 25
- Figure 2.1.** (a) The PXRD graph of ZIF-67 and  $V_{0.2}Co-LDH$ ; (b) shows the FTIR spectra of ZIF-67 and  $V_{0.2}Co-LDH$ ; (c) The Co 2p XPS spectra of Co-LDH and  $V_{0.2}Co-LDH$  showing the modulation of the electronic structure after the introduction of V in the structure of the catalyst. The \* marked peaks are satellite peaks of Co(II); (d) V 2p X-ray photoelectron spectrum of  $V_{0.2}Co-LDH$ . The V2p spectrum was deconvoluted into two peaks with binding energy 518.8 eV and 524.24 eV corresponding to V 2p<sub>1/2</sub> and V 2p<sub>3/2</sub> (e) The O 1s XPS was fitted into two peaks for the oxygen of -OH group, and Co/V-O bond. 41
- Figure 2.2.** (a-b) SEM image of ZIF-67 and  $V_{0.2}Co-LDH$ ; (b) TEM image showing the hollow nanocages of  $V_{0.2}Co-LDH$ ; (c) EDX of the catalyst showing presence of Co, V and O; (d-e) TEM image of  $V_{0.2}Co-LDH$ . 42
- Figure 2.3.** (a) LSV profiles for OER of  $V_xCo-LDH$  catalysts having different amount of V in the structure; (b) Tafel plots for the oxygen evolution reaction of  $V_{0.2}Co-LDH$  compared with other catalysts; The lowest Tafel slope for  $V_{0.2}Co-LDH$  was observed; (c) Comparative plots of the overpotentials and Tafel slopes for the catalysts showing the best activity and fastest kinetics for  $V_{0.2}Co-LDH$ ; (d) Determination of double-layer capacitance ( $C_{dl}$ ) of the as synthesized catalysts; (e) demonstrates Nyquist plots for the catalysts, obtained from electrochemical impedance spectroscopic (EIS) measurements showing lowest charge transfer resistance for  $V_{0.2}Co-LDH$ ; (f) chronoamperometric stability test of  $V_{0.2}Co-LDH$  and inset showing negligible change in the LSV profile after a 24 h long high current density chronoamperometric study. 44
- Figure 3.1.** (a) The PXRD graph of ZIF-67@NF, Co-LDH@NF and  $Fe_{0.4}Co-LDH@NF$ ; (b) shows the FTIR spectra of ZIF-67@NF, Co-LDH@NF and  $Fe_{0.4}Co-LDH@NF$ ; (c) The Co 2p XPS spectra of Co-LDH and  $Fe_{0.4}Co-LDH$  showing the modulation of the electronic structure after 58

the introduction of Fe(III) in the structure of the catalyst. The \* marked peaks are satellite peaks of Co(II); (d) Fe 2p X-ray photoelectron spectrum of Fe<sub>0.4</sub>Co-LDH. The Fe 2p spectrum was deconvoluted into two peaks with binding energy 724.15 eV and 710.61 eV corresponding to Fe 2p<sub>1/2</sub> and Fe 2p<sub>3/2</sub> (e) The O 1s XPS was fitted into three peaks for the oxygen of water (531.28 eV), surface oxygen (530.38 eV), and Co/Fe-O bond (529.38 eV).

**Figure 3.2.** (a) SEM image showing the uniformly grown nanosheets of Fe<sub>0.4</sub>Co-LDH@NF on nickel foam (inset ZIF-67); (b-e) Corresponding elemental mapping showing the uniform distribution of all the element; (f) TEM image showing the nanosheets of Fe<sub>0.4</sub>Co-LDH having an atomic level thickness; (g) TEM image showing the transparent nanosheets of Fe<sub>0.4</sub>Co-LDH, inset SAED pattern of Fe<sub>0.4</sub>Co-LDH; (h) HR-TEM image showing the d-spacing of 0.347, corresponding to the (006) plane of Fe<sub>0.4</sub>Co-LDH; (i) AFM image of Fe<sub>0.4</sub>Co-LDH@NF; (j) corresponding height profile showing the ~ 4 nm thickness of the nanosheets. The thin nanosheets offer a large number of active sites with coordinative and electronic unsaturation for substrate binding as well as high active surface area.

59

**Figure 3.3.** (a, b) LSV profiles for OER of Fe<sub>x</sub>Co-LDH@NF catalysts having different amount of Fe(III) in the structure; (c) Tafel plots of all synthesized catalysts for OER; (d) comparative plots of the overpotentials and Tafel slopes for the catalysts showing the best activity and fastest kinetics for Fe<sub>0.4</sub>Co-LDH@NF; (e) Comparison of the overpotential of the catalysts to reach a current density of 100 mA cm<sup>-2</sup>; (f) CV profiles of Fe<sub>0.4</sub>Co-LDH@NF and Co-LDH showing the redox peaks for the oxidation of Co<sup>II</sup> to Co<sup>III</sup> and Co<sup>III</sup> to Co<sup>IV</sup> during the OER; (g) demonstrates Nyquist plots for the Fe<sub>0.4</sub>Co-LDH@NF, Co-LDH@NF, ZIF-67@NF, Fe<sub>0.4</sub>Co-ZIF@NF, Fe<sub>0.4</sub>Co-HC@NF, and bare nickel foam obtained from electrochemical impedance spectroscopic (EIS) measurements showing lowest charge transfer

62

resistance for Fe<sub>0.4</sub>Co-LDH@NF. The spectra were collected with an anodic polarization potential of 1.48 V vs RHE; (h) chronoamperometric stability test of Fe<sub>0.4</sub>Co-LDH@NF and inset showing negligible change in the LSV profile after a 40 h long high current density chronoamperometric study.

**Figure 3.4.** Determination of double-layer capacitance ( $C_{dl}$ ) of Fe<sub>0.4</sub>Co-LDH, Co-LDH@NF, Fe<sub>0.4</sub>Co-HC@NF, Fe<sub>0.4</sub>Co-ZIF@NF and ZIF-67@NF by plotting (difference in current density)/2 against scan rate. **64**

**Figure 3.5.** (a) Plot of ECSA vs Catalyst Fe<sub>x</sub>Co-LDHs@NF. The plot shows that the ECSA is increased up to Fe<sub>0.4</sub>Co-LDH with increase in the iron substitution after that no increment in ECSA is observed; (b) The OER current density of different catalysts attained at 200 mV overpotential plotted against ECSA; (c) Potential vs current density plots showing the reduction peak used for the area integration curve; (d) The number of active sites of Fe<sub>x</sub>Co-LDH@NF having different amount of Fe(III); (e) Plot of the number of active sites vs ECSA for Fe<sub>x</sub>Co-LDHs@NF; (f) Plot for the turn over frequency (TOF) of catalysts Fe<sub>x</sub>Co-LDHs@NF. **65**

**Figure 4.1.** (a) The PXRD graph of ZIF-67@NF, and FeCo-LDH-3; (b) The Co 2p XPS spectra of Co-LDH-3 and FeCo-LDH-3 showing the changes in the electronic structure resulting from the incorporation of Fe(III) into the catalyst; (c) Fe 2p X-ray photoelectron spectrum of FeCo-LDH-3. The Fe2p spectrum was deconvoluted into two peaks with binding energy 723.59 eV and 710.55 eV corresponding to Fe 2p<sub>1/2</sub> and, Fe 2p<sub>3/2</sub>; (d) The O 1s XPS Co-LDH-3 and FeCo-LDH-3; (e) CV profiles of ZIF-67, Co-LDH-3, and FeCo-LDH-3 demonstrating the redox peaks for Co<sup>2+</sup>/Co<sup>3+</sup> couple. **78**

**Figure 4.2.** (a) SEM image of ZIF-67@NF; (b-c) SEM image of FeCo-LDH-3; (d-e) TEM image showing the formation of nanosheet FeCo-LDH-3; (f) HR-TEM image of FeCo-LDH-3; (g) EDX spectrum of **79**

electrochemically derived FeCo-LDH-3 showing the existence of Co, Fe and O elements.

- Figure 4.3.** (a) LSV profile of all electrochemically derived FeCo-LDH-x showing the excellent performance of FeCo-LDH-3; (b) Comparison of overpotential and current density of all active catalysts; (c) Tafel plots of all catalysts for OER; (d) Determination of double-layer capacitance ( $C_{dl}$ ) of various synthesized catalysts by plotting (difference in current density)/2 against scan rate; (e) demonstrates Nyquist plots for all catalysts obtained from electrochemical impedance spectroscopic (EIS) measurements showing lowest charge transfer resistance for FeCo-LDH-3; (f) Chronoamperometric measurement for the oxygen evolution reaction of FeCo-LDH-3 and Co-LDH-3 at 1.5 V vs RHE. The current density of Co-LDH-3 was found to decrease from the beginning due to the deactivation whereas FeCo-LDH-3 exhibited long term stability for 52 h. 82

- Figure 5.1.** (a) Top) The powder X-ray diffraction pattern of CeCo-2 shows two distinct sets of peaks, confirming the presence of two phases. Peaks labelled with \* correspond to CeO<sub>2</sub>, while peaks marked with ♦ indicate CeCo-LDH. Additionally, ♣ marks denote the presence of nickel foam; (b) The powder X-ray diffraction pattern of CeCo-2 and CeCo-LDH; (c) Fourier transformed infrared (FTIR) spectra of ZIF-67, Co-LDH and CeCo-2. Peak obtained at 1385 cm<sup>-1</sup> confirms the presence of intercalated carbonate anion between the layers of Ce-Co-LDH; (d) Co 2p XPS of Co-LDH is compared with that of CeCo-2; (e) Ce 3d XPS showing the presence of both Ce<sup>III</sup> and Ce<sup>IV</sup> species; (f) O 1s XPS spectrum was deconvoluted into three peaks corresponding to Co/Ce-O, hydroxyl species and oxygen defect sites. 92

- Figure 5.2.** (a) SEM image of CeCo-2 on nickel foam; (b) TEM image showing the ultrathin nanosheets of CeCo-2 having an atomic level thickness; (c) HR-TEM image showing the distribution of CeO<sub>2</sub> on CeCo-LDH; (d) HR- 95

TEM image showing the interface formation between CeO<sub>2</sub> and Co-LDH; (e)-(g) The lattice spacing corresponding to the region (1), (2) and (3) in the figure (d); (h)-(k) Elemental mapping of CeCo-2 showing the distribution of elements Ce, Co, C, and O; (l) The thickness of vertically grown CeCo-2 nanosheets; (m) HRTEM image showing the defect rich sites (green circle) in CeO<sub>2</sub> of CeCo-2; (c1)-(e1) FFT of the areas (1), (2), and (3) in the figure (d), respectively; (c2)-(e2) The corresponding inverse FFT images of (c1)-(e1), respectively; (c3)-(e3) The contrast intensity profiles corresponding to the figures (c2)-(e2) showing the lattice parameters.

**Figure 5.3.** (a) CV profiles of CeCo-2 and Co-LDH displaying redox peaks corresponding to the oxidation of Co<sup>II</sup> to Co<sup>III</sup> and Co<sup>III</sup> to Co<sup>IV</sup> during the OER; (b) Linear sweep voltammetric profiles of the OER for the synthesized catalysts, illustrating enhanced catalytic activity upon Ce introduction into Co-LDH, with CeCo-2 demonstrating the highest activity; (c) Comparative plots of overpotentials and current density for different catalysts, demonstrating CeCo-2's superior performance; (d) LSV profiles for OER of the synthesized catalysts compared to the benchmark catalyst RuO<sub>2</sub>, highlighting CeCo-2's superior activity; (e) Tafel plots for the oxygen evolution reaction comparing CeCo-2 with other catalysts. The lowest Tafel slope observed for CeCo-2 indicates the fastest OER kinetics; (f) Nyquist plots for CeCo-2, Co-LDH, CeCo-1, and CeCo-3, revealing the lowest charge transfer resistance for CeCo-2. Spectra were collected at an anodic polarization potential of 1.48 V vs RHE, within a frequency range of 0.01 to 10<sup>6</sup> Hz; (g) Determination of double-layer capacitance (C<sub>dl</sub>) for Co-LDH, CeCo-1, CeCo-2, and CeCo-3 by plotting (difference in current density)/2 against scan rate; (h) Long-term chronoamperometric OER performance of CeCo-2.

97

**Figure 5.4.** (a) The ECSA of the catalysts increased with higher Ce content, reaching a peak for CeCo-2 and decreasing with further increases in Ce(III); (b) Normalized current density based on ECSA for the catalysts;

100

(c) Plot of ECSA-normalized current density at 1.59 V, demonstrating CeCo-2 as the most active catalyst; (d) Potential versus current density plots showing the reduction peak used for area integration; (e) Calculation of the number of active sites for the catalysts; (f) Plot showing the turnover frequency (TOF) of the catalysts.

**Figure 5.5.** (a) LSV curves of CeCo-2 before and after CA, (b) PXRD of CeCo-2 after 100 h CA measurement, and (c-d) SEM images of CeCo-2 after 100 h CA measurement; (e) Schematic representation of  $\pi$ -orbital overlap to promote electron transfer from  $\text{Co}^{\text{II/III}}$  to  $\text{Ce}^{\text{IV}}$  involving O (2p)  $\pi$ -orbital. **102**

# List of Schemes

---

<b>Scheme No.</b>	<b>Title</b>	<b>Page No.</b>
<b>Scheme 2.1</b>	Schematic diagram showing the synthesis of $V_xCo$ -LDH from ZIF-67	<b>37</b>
<b>Scheme 3.1</b>	Schematic diagram showing the synthesis of cobalt hydroxide carbonate (Co-HC) templated ZIF-67	<b>52</b>
<b>Scheme 4.1</b>	Schematic representation showing the conversion of precatalyst ZIF-67@NF into active catalyst FeCo-LDH-3 under cyclic voltametric condition.	<b>75</b>
<b>Scheme 5.1</b>	Scheme 1 Schematic diagram showing the transformation of ZIF-67 into $CeCo-x$ ( $x = 1, 2, 3$ ) by a Lewis acid $Ce^{III}$ -assisted hydroxylation	<b>88</b>

# List of Table

---

<b>Table No.</b>	<b>Title</b>	<b>Page No.</b>
<b>Table 2.1.</b>	Details of various synthesized $V_xCo$ -LDH catalysts.	<b>40</b>
<b>Table 2.2.</b>	The OER activities of reported LDHs compared with $V_{0.2}Co$ -LDH.	<b>45</b>
<b>Table 3.1.</b>	Details of all synthesized $Fe_xCo$ -LDH catalysts.	<b>57</b>
<b>Table 3.2.</b>	The OER activities of reported LDHs compared with $Fe_{0.4}Co$ -LDH@NF.	<b>63</b>
<b>Table 3.3.</b>	The determination of $C_{dl}$ and ECSA of $Fe_xCo$ -LDH.	<b>66</b>
<b>Table 3.4.</b>	Area under the curve, no. of active site and turnover frequency of $Fe_xCo$ -LDH catalyst.	<b>67</b>
<b>Table 3.5.</b>	The OER activities of ZIF derived electrocatalysts compared with $Fe_{0.4}Co$ -LDH@NF.	<b>68</b>
<b>Table 4.1.</b>	Details of active catalysts synthesized by the electrochemical transformation of ZIF-67 and their reaction condition.	<b>77</b>
<b>Table 4.2.</b>	Comparison of electronic interaction between Co and Fe in $FeCo$ -LDH-3 and $Fe_{0.4}Co$ -LDH.	<b>79</b>
<b>Table 4.3.</b>	Comparison of OER activities of reported LDHs and $FeCo$ -LDH-3.	<b>81</b>
<b>Table 4.4.</b>	Comparison of OER activities of electrochemically synthesized $FeCo$ -LDH-3, $Co$ -LDH-3 and hydrothermally synthesized $Fe_{0.4}Co$ -LDH and $Co$ -LDH.	<b>83</b>
<b>Table 5.1.</b>	Details of the synthesis of $CeCo$ -x catalysts.	<b>91</b>
<b>Table 5.2.</b>	The OER activities of reported electrocatalysts compared with $CeCo$ -2.	<b>98</b>
<b>Table 5.3.</b>	The determination of $C_{dl}$ and ECSA for different catalysts.	<b>100</b>

<b>Table 5.4.</b>	ECSA normalized OER activity of reported catalysts compared with CeCo-2.	<b>101</b>
<b>Table 5.5.</b>	Number of active sites and TOFs of different catalysts.	<b>102</b>
<b>Table 6.1.</b>	Details of all catalysts synthesized in this thesis work.	<b>109</b>

## List of Symbols/Abbreviations

---

$\theta$	Angle (degree)
a.u.	Atomic Unit
BE	Binding Energy
eV	Electron Volt
EDX	Energy Dispersive X-ray
HR-SEM	High Resolution-Scanning Electron Microscopy
MOF	Metal-Organic Framework
SAED	Selected Area Electron Diffraction
s	Second
HR-TEM	High Resolution-Transmission Electron Microscopy
XPS	X-ray Photoelectron Spectroscopy
XRD	X-ray Diffraction
$\lambda$	Wavelength
ZIF	Zeolitic Imidazolate Framework
$\eta$	Overpotential
$\Omega$	Ohm
j	Current Density
ECSA	Electrochemical Active Surface Area
$S_{\text{Ageo}}$	Geometrical Surface Area
$C_{\text{dl}}$	Double-Layer Capacitance
LDHs	Layered Double Hydroxides
$R_{\text{ct}}$	Charge Transfer Resistance
TOF	Turn Over Frequency

<b>NF</b>	<b>Nickel foam</b>
<b>EIS</b>	<b>Electrochemical Impedance Spectroscopy</b>
<b>CV</b>	<b>Cyclic Voltammetry</b>
<b>LSV</b>	<b>Linear Sweep Voltammetry</b>
<b>RHE</b>	<b>Reversible Hydrogen Electrode</b>
<b>OER</b>	<b>Oxygen Evolution Reaction</b>
<b>HER</b>	<b>Hydrogen Evolution Reaction</b>
<b>CA</b>	<b>Chronoamperometry</b>
<b>PBA</b>	<b>Prussian Blue Analogue</b>
<b>MIL</b>	<b>Materials of Institute Lavoisier</b>
<b>SDS</b>	<b>Sodium Dodecyl Sulfate</b>
<b>AFM</b>	<b>Atomic Force Microscopy</b>